**Proceedings of the ASME 2022 41st International Conference on Ocean, Offshore and Arctic Engineering**
**OMAE 2022**
**June 5–10, 2022, Hamburg, Germany**

# OMAE2022-80990

# ENERGY-MAXIMISING CONTROL PHILOSOPHY FOR A CYCLOROTOR WAVE ENERGY DEVICE

**John V. Ringwood***
Centre for Ocean Energy Research
Maynooth University, Ireland
Email: john.ringwood@mu.ie

**Andrei Ermakov**
Centre for Ocean Energy Research
Maynooth University, Ireland
Email: andrei.ermakov@mu.ie

## ABSTRACT

Recently, cyclorotors, utilizing lift rather than buoyancy forces for energy extraction, have been proposed and inherit many of the appealing features characteristic of modern wind turbines. In particular, the ability to spill energy though foil pitching allows the device to remain at rated power despite significant variations in input power level, while additional cyclorotor features, including variable submergence depth and rotor radius, also permit a significant degree of modulation of the device structure, and energy absorption characteristics, offering considerable flexibility. These configuration flexibilities, in addition to torque control of the rotor/generator shaft (also characteristic of wind turbines) offers the control engineer considerable freedom in adjusting the device characteristics to maximise the effectiveness of the device in capturing wave power, while maintaining structural integrity and minimizing harmful stresses on system components. However, such flexibility also provides a significant challenge in the form of a multivariable control problem for a system described by significantly nonlinear hydrodynamics. This paper describes a proposed hierarchical control system for a cyclorotor wave energy device, utilizing submergence depth, rotor radius, foil pitch angles, and shaft torque as control inputs. The hierarchy involves the separation of the control actuators into two classes: structural (or slow) control effectors, and wave-by-wave (or fast) control effectors. In particular, the paper will examine the interaction between the two levels of the control hierarchy and the need, if any, for simultaneous optimisation of the control parameters at both levels.

## KEYWORDS

Renewable energy; wave energy converter; control system; cyclorotor; hierarchical control; LiftWEC; lift-based wave energy converter;

## 1 INTRODUCTION

It is widely accepted that energy-maximising control systems are crucial to maximise the economic performance of wave energy converters, with expectations of doubling of captured power in realistic (irregular) waves [1]. However, the means by which control actions are implemented, and wide variety in the range of concepts, principles, and structural geometry associated with WEC technology, preclude the possibility for a generic approach to energy-maximising control of wave energy converters. In general, for heaving point absorbers, flaps and other diffraction/buoyancy-activated devices, the typical control input is the force (or torque) realised by the power take-off (PTO) system in resisting the motion of the device [2]. The PTO, therefore, is the system component which converts the wave energy converter (WEC) motion into useful energy. The PTO normally consists of a linear or rotational generator as the final element, with a potential intermediate hydraulic stage to convert the high force/low speed motion into higher speed motion (with the potential addition of motion rectification) preferred by electrical machinery.

Cyclorotors, which can have a variety of forms [3], generally permit a range of control mechanisms, which operate on a variety of timescales, harnessing hydrodynamic lift forces [4], rather than diffraction/buoyancy forces. This presents both a significant opportunity to optimise power capture [5–7], but also a challenge in managing the multivariable nature of the control problem. To

*Address all correspondence to this author.

date, some progress has been recorded in control studies on cyclorotors, with initial analysis and experimental results carried out by Hermans et al [8], Scharmann [9] and the Atargis Energy Corporation [10–13]. These pioneering studies focus on wave cancellation as a control performance metric and used a constant cyclorotor rotational speed. More recently, some studies have shown the benefit of a variable rotational velocity, and the use of shaft power as a primary performance metric [14]. Specific studies [15] examined the use of both relatively fast acting (generator torque, foil pitch angles), and slow acting (submergence depth, rotor radius) control actuators have recently emerged, showing potential improvement in power capture of over 100%,

Given the disparity of time scales over which control actuators can operate, to date there has been no analysis of the interaction between these different actuator sets on the system performance. To that end, this paper performs a preliminary sensitivity analysis, which examines the need for co-optimality between control effectors operating on different time scales. This leads to a (temporal) control hierarchy, which provides a suitable framework for the analysis of interaction effects. A minor contribution of the paper is the consideration, from a qualitative perspective, of the impact of various control actions on device structural health, as well as some more general economic considerations.

The remainder of the paper is organised as follows: Section 2 details the cyclorotor system, showing the control effectors and also providing a schematic which documents the manipulated (control) variables. Section 3 outlines the validated system model which is used for evaluation and control optimisation calculations, while Section 4 documents the control metrics and the real-time control parameterisations employed. The core results of the paper are developed in Section 5, which include some sample time-domain results, but focus mainly on the sensitivity interactions between the fast and slow control actuators. Finally, conclusions are drawn in Section 6.

## 2 CYCLOROTOR SYSTEM

### 2.1 System description

The cyclorotor system is shown in Fig.1. Note that, while Fig.1 shows a 2-foil rotor, a different number of foils could be used, though the vast bulk of cyclorotors tested to date have either one or two foils [9, 10]. From Fig.1, four manipulated (control) variables are evident: Submergence depth $D_s$, rotor radius $R$, foil pitch angle $\gamma$, and generator torque $\mathscr{T}$. We assume the optimal relation between hydrofoil chord $C$ and operational radius $R$ as $C = 0.8R$, which has been established in [16]. For a two-foil system, we will assume that the foils have opposite pitch angles i.e. $\gamma_1 = -\gamma_2 = \gamma$ [13], resulting in just a single foil angle control input $\gamma$.

### 2.2 Control system hierarchy

The current approach [15] to the manipulation of the various control effectors, in an effort maximise power capture, is

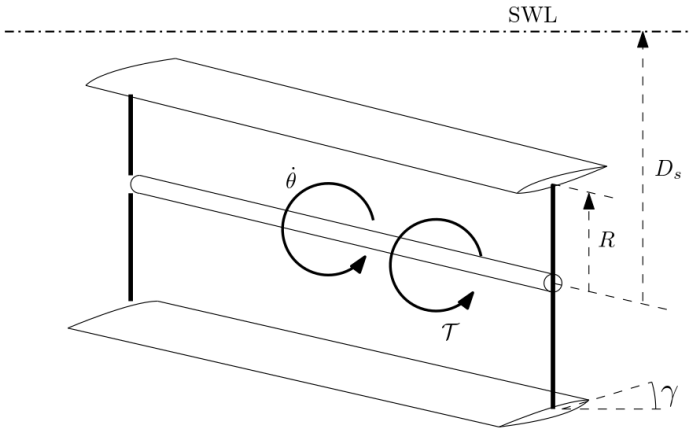


**FIGURE 1**. Schematic of a 2-foil cyclorotor system system, showing the various manipulated variables of submergence depth $D_s$, rotor radius $R$, foil pitch angle $\gamma$, and generator torque $\mathscr{T}$. $\dot{\theta}$ denotes the rotor angular velocity. SWL denotes the still water level.

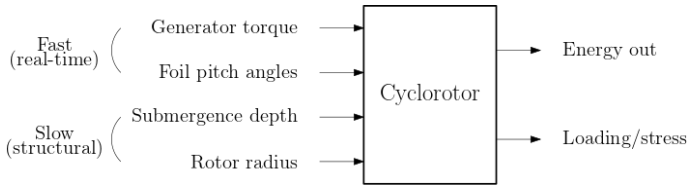


**FIGURE 2**. System block diagram, showing the range of manipulated variables (inputs) and target quantities (outputs).

somewhat 'sequential' in terms of the optimisation strategy, as shown in Fig.3. The sequential procedure can be summarised as follows:

1. The performance metric is the converted (shaft) energy.
2. Assuming a constant rotational speed, and a neutral foil pitch angle, the submergence depth $D_s$ and rotor radius $R$ are optimised.
3. The evolution of real-time pitch angle $\gamma$ and angular velocity $\dot{\theta}$ are now parameterised in terms of Fourier series and the optimal Fourier coefficients determined to maximise converted energy.

We note that the procedure above can be carried out for both monochromatic and panchromatic incident waves. This sequential procedure provokes two important questions:

(a) Are $D_s$ and $R$ now optimal, considering that $\gamma$ and $\dot{\theta}$ are not constant, and
(b) What is the effect of a non-optimal $D_s$ and $R$ on the optimal evolution of $\gamma$ and $\dot{\theta}$?

Issue (a) above relates to the fact that the optimisation procedure in Fig.3 is sequential from top to bottom, while (b) relates to the possibility of local optima for $D_s$ and $R$, or the (inevitable) presence of errors in the model of Section 3[1].

[1]However, we note that, in general, the model of Section 3 validates well against previously published experimental data [17] though, of course, no model is perfect.

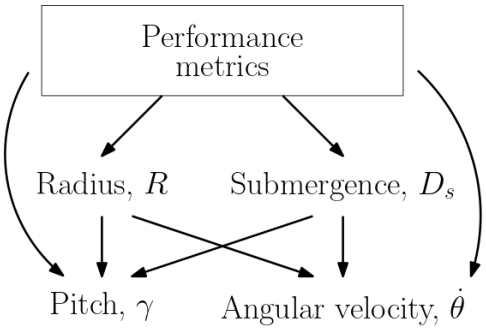


**FIGURE 3**. Previous control optimisation strategy, showing sequential process

## 3 Outline of system model

We model the hydrofoils using a point-source representation [18, 19], with the corresponding equations validated against experimental results obtained by previous studies [8, 11, 12] in terms of waves radiated by a rotor, and assuming a 2D hydrofoil thin chord profile. In the 2D model, we consider the side profile of the cyclorotor, with the output power expressed in Watts per meter of foil width (W/m). The results of the free rotor rotation in waves, obtained with the use of a point source model, are presented in [17].

In the point source model, it is assumed that the lift, drag and tangential forces are caused by the interaction of the rotation of hydrofoil $i$ with an overall relative velocity $\hat{\mathbf{V}}_\mathbf{i}$, representing the vector difference between the wave induced fluid velocity $\mathbf{V}_{\mathbf{W_i}}$ and the instantaneous (rotational) velocity of foil $i$ $\mathbf{V}_{\mathbf{R_i}}$, plus the sum of the wakes left by the moving foils $\mathbf{V}_{\mathbf{HW_{i,j}}}$, and the instantaneous radiation from the other foils $\mathbf{V}_{\mathbf{HM_j}}$ as:

$$\hat{\mathbf{V}}_\mathbf{i} = \mathbf{V}_{\mathbf{W_i}} - \mathbf{V}_{\mathbf{R_i}} + \mathbf{V}_{\mathbf{HWi}} + \mathbf{V}_{\mathbf{HMj}} + \mathbf{V}_{\mathbf{HWj}} \tag{1}$$

The rotational velocity components $\mathbf{V}_{\mathbf{R_i}}$ for foil $i$ can be found as the partial time derivatives of the hydrofoil positions $(x_i, y_i)$ where:

$$x_i(t) = R\cos(\theta(t) + \pi i) \tag{2}$$
$$y_i(t) = y_0 - R\sin(\theta(t) + \pi i) \tag{3}$$

with $\theta(t)$ being the position of the hydrofoil in polar coordinates. In this research, we consider the operational radius of the rotor $R$, the rotational rate $\dot{\theta}(t)$, submergence depth of the rotor centre $D_s$, and the (related) hydrofoil pitch angles $\gamma_i$ ($\gamma$) as the parameters which must be optimised for specific sea states. Note that, in this representation, pitch angle $\gamma$, submergence depth $D_s$ and rotor radius $R$ are set as independent parameters, while motor torque $\mathscr{T}$ is used as the manipulated variable in the closed loop control of velocity $\dot{\theta}$. A detailed explanation of the optimisation problem, as currently dealt with in [15], is presented as a block-scheme in Fig.3. In the following, we briefly present some general equations of the point source model to highlight the nonlinear influence of the optimisation parameters on tangential force generation and the performance metrics of the rotor. For a fuller treatment, the reader is referred to [17–19].

The velocity components $\mathbf{V_W}$ of the wave-induced water particle movements can be found as the partial derivative of the potential, using the corresponding coordinate. For example, for the case of the Airy potential, the velocity components can be found as a gradient:

$$\Phi_W = \frac{Hg}{2\omega} e^{ky} \sin(kx - \omega t) \tag{4}$$

$$\mathbf{V_W} = \nabla \Phi_W \tag{5}$$

where $H$ is the height, $\omega$ is the frequency and $k$ is the wave number of the incoming wave, with $g$ being gravitational acceleration. The velocity components of the waves radiated by the moving point source can be described by the following formula:

$$\mathbf{V_H} = \frac{\partial \mathscr{F}(\mathbf{z}, \mathbf{t})}{\partial \mathbf{z}} = (\mathbf{V_H})_\mathbf{x} - \mathbb{i}(\mathbf{V_H})_\mathbf{y} \tag{6}$$

which can be separated into the instantaneous radiated waves $\mathbf{V_{HM}}$ and wakes $\mathbf{V_{HW}}$ which are left in the hydrofoil's path:

$$\mathbf{V_H} = \mathbf{V_{HM}} + \mathbf{V_{HW}} \tag{7}$$

The waves generated by the hydrofoils are described by the use of the complex potential, derived in [18, 19], as:

$$\mathscr{F}(z,t) = \frac{\Gamma(t)}{2\pi\mathbb{i}} Log\left[\frac{z - c(t)}{z - \tilde{c}(t)}\right] - \frac{2\mathbb{i}\sqrt{g}}{\pi} \int_0^t \frac{\Gamma(\tau)}{\sqrt{\mathbb{i}(z - \tilde{c}(\tau))}} D\left[\frac{\sqrt{g}(t-\tau)}{2\sqrt{\mathbb{i}(z - \tilde{c}(\tau))}}\right] d\tau \tag{8}$$

where $z = x + \mathbb{i}y$ is the coordinate on the complex plane, $c(t) = x(t) + \mathbb{i}y(t)$ is the position of the hydrofoil, and $D(x)$ is the Dawson function [20]:

$$D(x) = e^{-x^2} \int_0^x e^{y^2} dy. \tag{9}$$

The velocity potential $\Phi_H$ of the waves radiated by the moving foils can then be found from the following relation:

$$\Phi_H(x,y) = Re[\mathscr{F}(z,t)] \tag{10}$$

Note that the tangential forces $F_T$ depend on the lift and drag coefficients $C_L(\alpha)$ and $C_D(\alpha)$, respectively, the chord length of the hydrofoil $C$, the water density $\rho$, and the overall hydrofoil/fluid relative velocity $\hat{\mathbf{V}}$ at the current hydrofoil position $(x_i, y_i)$:

$$F_T = \frac{1}{2}\rho(C_L(\alpha)\sin(\alpha-\gamma) - C_D(\alpha)\cos(\alpha-\gamma))|\hat{V}|^2 C \quad (11)$$

where $\gamma$ is the optimal *constant* hydrofoil pitch angle and $\alpha$ is the attack angle.

## 4 Control calculations

As described in Section 2, the control effectors operate on various time scales with, in general, the structural control parameters only changed in relation to sea state variations, due to their slow rate of movement. In contrast, changes in foil pitch angle and (especially) shaft/generator torque can be implemented on an inter-wave or intra-wave basis. To achieve maximum cyclorotor energy conversion performance, all control inputs must be, ideally, simultaneously optimised.

### 4.1 Performance metrics

It has been shown [15] that, in the case of a cyclorotor WEC, which rotates in monochromatic waves with the same phase and rotational rate as the waves, all hydrodynamic and mechanical processes became periodic after $K \sim 10$ rotational periods, at time instant $T_K$. Thus, the mechanical energy which can be generated, during one stable period between $T_K$ and $T_{K+1}$ seconds, in monochromatic waves, in terms of shaft power, has the following form:

$$\frac{R}{T}\int_{T_K}^{T_{K+1}} (F_{T_1} + F_{T_2})\,\dot{\theta}(t)dt \quad (12)$$

where $T_K$ represents wave period $K$. In the case of panchromatic waves, the periodic solution of [15] is not appropriate, and the influence of the moment of inertia $I$ of the rotor must also be taken into account, since $\dot{\theta}(T_{K+1}) \neq \dot{\theta}(T_K)$. The optimisation also must start after the moment $T_0$ when the complex (caused by rotation) velocity field has formed in the vicinity of the rotor. Then, for the case of panchromatic waves, the shaft power functional has the following form:

$$\frac{1}{(T-T_0)}\int_{T_0}^{T} \left((F_{T_1} + F_{T_2})R - I\ddot{\theta}(t)\right)\dot{\theta}(t)dt \quad (13)$$

### 4.2 Harmonic control solution

A solution for variable rotational rate $\dot{\theta}(t)$ and hydrofoil pitch angle $\gamma(t)$ in the form of a Fourier series (for the monochromatic wave case) is proposed:

$$\begin{bmatrix}\dot{\theta}(t)\\ \gamma(t)\end{bmatrix} = \begin{bmatrix}\omega\\ \gamma_0\end{bmatrix} + \sum_{i=1}^{m}\begin{bmatrix}a_i\\ \hat{a}_i\end{bmatrix}\cos\left(\frac{2\pi t}{T}i\right) + \begin{bmatrix}b_i\\ \hat{b}_i\end{bmatrix}\sin\left(\frac{2\pi t}{T}i\right) \quad (14)$$

where $(a_i, b_i)$ and $(\hat{a}_i, \hat{b}_i)$ are the amplitude coefficients of the harmonic terms corresponding to the time domain expression for rotational rate $\dot{\theta}(t)$ and hydrofoil pitch angle $\gamma(t)$, respectively, expressed as variations around the nominal values of $\omega$ and $\gamma_0$, respectively, with $\omega$ being the (monochromatic) wave frequency. Note that the variational representation eases the optimisation problem for the unknown $(a_i, b_i)$ and $(\hat{a}_i, \hat{b}_i)$, since the solution of (14) is already in the region of the global optimum.
For the case of panchromatic waves,

$$\begin{bmatrix}\dot{\theta}(t)\\ \gamma(t)\end{bmatrix} = \begin{bmatrix}\dot{\theta}_0\\ \gamma_0\end{bmatrix} + \sum_{i=1}^{m}\begin{bmatrix}a_i\\ \hat{a}_i\end{bmatrix}\cos\left(\frac{2\pi t}{T_{ext}}i + \begin{bmatrix}c_i\\ \hat{c}_i\end{bmatrix}\right) + \begin{bmatrix}b_i\\ \hat{b}_i\end{bmatrix}\sin\left(\frac{2\pi t}{T_{ext}}i + \begin{bmatrix}d_i\\ \hat{d}_i\end{bmatrix}\right) \quad (15)$$

where the additional phase offset terms $(c_i, \hat{c}_i)$ and $(d_i, \hat{d}_i)$ are included beyond (14) and the monochromatic wave frequency $\omega$ is replaced with a nominal rotational speed $\dot{\theta}_0$, which is the optimum (constant) rotational rate for the fundamental period $[T_0, T]$, again with the intention of easing the global optimisation problem. $T_{ext}$, in (15), is an extended time interval selected as twice the interval on which we consider the energy generation $[T_0, T]$. This condition permits a non-periodic solution, over the limited solution domain.

The problem of simultaneous identification of the optimal series coefficients for real time control strategies (14), (15) and structural parameters $D_s$, $R$ is solved using a Python implementation of simplicial homology global optimisation and differential evolution [21, 22]. The convergence of this spectral method has already been demonstrated in [14, 15].

It is assumed that we can estimate the properties of the incoming wave-induced wave particle velocities over the next 10 seconds, using measurements from an acoustic Doppler velocimeter (ADP) and an estimation algorithm developed by the Atargis Energy Corporation [23].

In order to provide sufficient control freedom, the constraint on the main shaft torque is selected as $|\mathscr{T}| < 2\cdot 10^7\ Nm$. Variations in the rotation rate $\tilde{\omega} = \dot{\theta}/\omega$ are also limited to $1/2 < \tilde{\omega} < 2$, to satisfy realistic electrical machine capabilities, while excursions in pitch angle are limited to $|\gamma'(t)| < 15^o s^{-1}$ to avoid significant hydrodynamic pressure on the hydrofoils.

## 5 Cyclorotor optimisation results

In this section, the various manipulated variables of the cyclorotor are optimised, for the case of monochromatic and

panchromatic waves, maximising the performance metrics of (12) and (13), respectively. In particular, we focus on two issues:

a The degree to which $R$ and $D_s$, optimised for a constant rotational rate $\dot{\theta}$ and pitch $\gamma$ (as in [15]), are still optimal under variable $\dot{\theta}$ and $\gamma$, and
b The sensitivity of the system performance, and optimal solutions for $\dot{\theta}$ and $\gamma$, to mismatch in optimal $R$ and $D_s$.

### 5.1 Monochromatic waves

In this subsection, we study the optimal structural design and control strategies for a cyclorotor-based WEC, operating in monochromatic waves with $T$=10s and $H$=2m, with power $P_{Wave}$ = 38.3 kW/m. The performance of the cyclorotor is assessed in kW of mechanical power, per meter of cyclorotor shaft length (i.e. kW/m).

**5.1.1 Constant $\dot{\theta}$ and $\gamma$** As a baseline case, the structural optimisation of a cyclorotor with two hydrofoils NACA0015 [24], with a constant rotational rate matched with the incoming wave frequency $\dot{\theta} = \omega$, is examined in Table 1, considering the simplest case of a neutral pitch angle of $\gamma = 0^o$. Note the sensitivity of the converted mean power to variations in $D_s$ and $R$, with an optimum $R$ of 7.5m and as shallow a depth as possible (subject to interaction with surface effects).

A slightly more complex case now utilises a constant pitch angle $\gamma$ which maintains, on average, an optimum $\gamma$ corresponding to a constant rotational rate [13] stall angle of attack $\alpha_i = 15^o$ between the rotor foils and the movement of the surrounding water particles. Even with a constant $\gamma$, the employment of an optimal (constant) pitch angle has the effect of almost doubling the mean converted power (compared to the neutral pitch case), as shown in Table 2, with the corresponding optimal pitch values shown in Table 3. Apart from the significant increase in converted mean power, other characteristics of Tables 2 and 3 are noteworthy:

(a) The optimal radius $R$ is still 7.5m,
(b) The optimum submergence depth $D_s$, in general, is still minimal, though a slightly larger depth is preferred around the optimum power capture point,
(c) The sensitivity of $P_{Shaft}$ to variations in $D_s$ is significantly reduced, and
(d) The optimal pitch angle (from Table 3) is not especially sensitive to reductions in $R$ below its optimal value, but is sharply sensitive to increases.

**5.1.2 Variable $\dot{\theta}$ and $\gamma$** Still using monochromatic waves, the solution in (14) is now optimised against the performance criterion in (12). By way of example, for $m = 12$ harmonics, the time domain solution for $\dot{\theta}$ and $\gamma$ is shown in Fig.4. It can be noted that, similarly to the results obtained in [15], there is significant variation in both $\dot{\theta}$ and $\gamma$, with $\dot{\theta}$ values of up to twice the wave frequency and $\gamma$ values varying up to 50% from

**TABLE 1**. Performance (kW/m), in terms of shaft power $P_{Shaft}$, for a twin-foil cyclorotor with a constant neutral pitch angle $\gamma = 0^o$ and constant rotational rate $\dot{\theta} = \omega$, for various values of submergence depth $D_s$ and radius $R$, in monochromatic waves with $T$ = 10s and $H$= 2m.

| $D_s(m) \setminus R(m)$ | 4.5 | 5.5 | 6.5 | 7.5 | 8.5 |
|---|---|---|---|---|---|
| 12.75 | 7.17 | 9.4 | 11.18 | 12.1 | 11.85 |
| 13.75 | 6.68 | 8.82 | 10.53 | 11.47 | 11.3 |
| 14.75 | 6.21 | 8.23 | 9.86 | 10.78 | 10.7 |
| 15.75 | 5.77 | 7.66 | 9.2 | 10.06 | 9.93 |
| 16.75 | 5.35 | 7.11 | 8.54 | 9.34 | 9.18 |

**TABLE 2**. Performance (kW/m), in terms of shaft power $P_{Shaft}$, for a twin-foil cyclorotor with optimal constant pitch angle $\gamma = \gamma_{opt}$ (see Table 3 for values) and constant rotational rate $\dot{\theta} = \omega$, for various values of submergence depth $D_s$ and radius $R$, in monochromatic waves with $T$ = 10s and $H$ = 2m.

| $D_s(m) \setminus R(m)$ | 4.5 | 5.5 | 6.5 | 7.5 | 8.5 |
|---|---|---|---|---|---|
| 12.75 | 12.6 | 19.95 | 25.79 | 26.12 | 24.4 |
| 13.75 | 12.14 | 19.38 | 25.61 | 26.8 | 24.46 |
| 14.75 | 11.69 | 18.78 | 25.21 | 27.26 | 24.81 |
| 15.75 | 11.25 | 18.17 | 24.68 | **27.42** | 25.28 |
| 16.75 | 10.82 | 17.55 | 24.08 | 27.36 | 25.75 |

**TABLE 3**. Values of optimal constant pitch angles $\gamma_{opt}$ [deg] corresponding to Table 2, in monochromatic waves with $T$ = 10s and $H$ = 2m.

| $D_s(m) \setminus R(m)$ | 4.5 | 5.5 | 6.5 | 7.5 | 8.5 |
|---|---|---|---|---|---|
| 12.75 | 8.75 | 10.45 | 11.5 | 9.55 | 6.57 |
| 13.75 | 8.91 | 10.53 | 11.6 | 10.48 | 6.96 |
| 14.75 | 9.06 | 10.6 | 11.58 | 11.09 | 7.55 |
| 15.75 | 9.21 | 10.67 | 11.54 | 11.14 | 8.28 |
| 16.75 | 9.36 | 10.69 | 11.5 | 11.3 | 8.49 |

**TABLE 4**. Performance (kW/m), in terms of shaft power $P_{Shaft}$, for a twin-foil cyclorotor with variable pitch angle $\gamma$ and variable rotational rate $\dot{\theta}$, for various values of submergence depth $D_s$ and radius $R$, in monochromatic waves with $T$ = 10s and $H$ = 2m.

| $D_s(m) \setminus R(m)$ | 4.5 | 5.5 | 6.5 | 7.5 |
|---|---|---|---|---|
| 12.75 | 15.94 | 25.17 | 38.24 | 38.3 |
| 13.75 | 15.09 | 24.73 | 37.1 | 38.3 |
| 14.75 | 14.4 | 22.47 | 36.26 | 38.3 |
| 15.75 | 13.82 | 23.04 | 33.83 | 38.3 |
| 16.75 | 12.91 | 22.97 | 32.8 | 38.3 |

the constant optimal value. We can also note that considerable utility is made of the higher harmonics, with there being no obvious profile matches between the evolution of $\dot{\theta}$ and $\gamma$ compared to the evolution in the free surface. This is in sharp contrast to the case for more traditional buoyancy/diffraction-based WECs where, under optimal conditions, a strong correlation between wave excitation force (closely related to the free surface profile) and the device velocity exists [2]. Note also that the use of higher harmonics in hydrofoil pitch angle are not so significant (due to the simple circular motion of the wave particles), but the rotational rate switches between available maximum and minimum values. While marginally higher $P_{Shaft}$ values can be obtained for larger values of $m$, the use of more harmonics also brings higher stresses, and stress frequencies/rates, on the system structure.

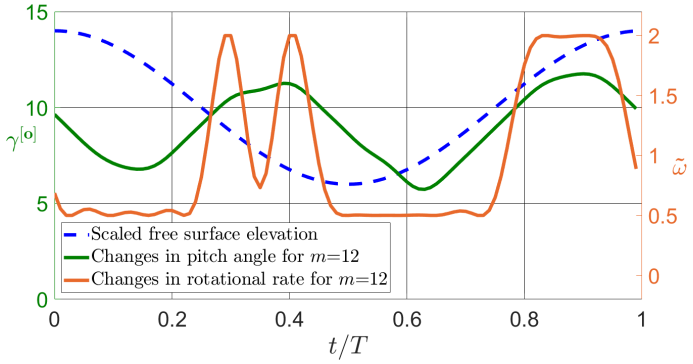


**FIGURE 4**. Example time-domain solution for variable pitch and rotational rate for a cyclorotor with radius $R$=5m and submergence $D_s$=15m in monochromatic waves with $T$=10s and $H$=2m. The rotor generates $P_{Shaft}$=19.66kW/m with the use of $m = 12$ harmonics.

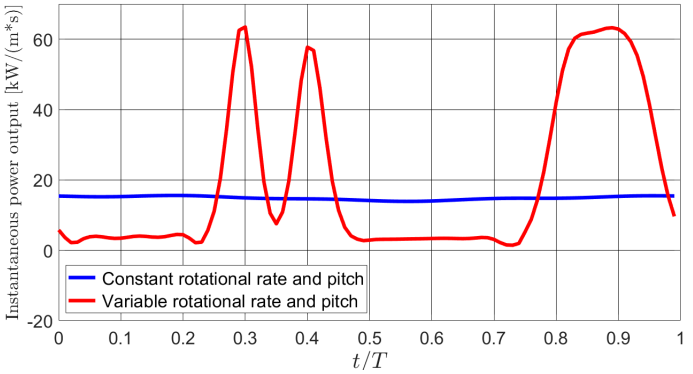


**FIGURE 5**. Increase in instantaneous power generation after implementation of the control strategy presented in Fig. 4, showing the significant improvement under variable pitch and rotational rate.

Table 4 shows the sensitivity of the converted mean power to variations in radius $R$ and submergence depth $D_s$, where both $\dot{\theta}$ and $\gamma$ are allowed to vary with time. A key aspiration here is to see if optimal $R$ and $D_s$ values calculated for the constant $\dot{\theta}$ and $\gamma$ case are still optimal for the variable $\dot{\theta}$ and $\gamma$ case. Specifically, Table 4 shows that the optimal radius of 7.5m is still preferred (within the range of $R$ examined), with any sensitivity to the depth being minimal. We note that it would be challenging to construct real-world rotors of radius approaching 10m, due to the significant structural loads involved [16].

## 5.2 Panchromatic waves

In this subsection, the optimal (combined) structural design and control strategy, for a cyclorotor-based WEC operating over a 10 s time interval of panchromatic waves with $H_s$=1.5m and $T_e$=8s is examined. The average power of such a panchromatic wave is $P_{Wave}$=8.3kW/m. The moment of inertia $I$ of the cyclorotor, which plays a role in the panchromatic case [15], is proportional to its radius $R$ and chord length $C$ and the following approximation:

$$I = 2 * R^2 * C * M \tag{16}$$

where $M = 2kg/m^2$ is the mass of one square metre of foil surface, is employed.

The optimal structural design $R, D_s$ of a cyclorotor with two hydrofoils NACA0015 [24], with a constant pitch angle $\gamma_0 = 0$ and constant optimal rotational rate $\dot{\theta}_0$, for the same panchromatic wave $Hs$ = 1.5m and $Te$ = 8s, is studied in [15]. In this current study, however, we solve the problem of the *simultaneous* optimisation of the cyclorotor geometry $R, D_s$ and *real-time* control strategy for variable rotational rate $\dot{\theta}$ and variable pitch angle $\gamma$.

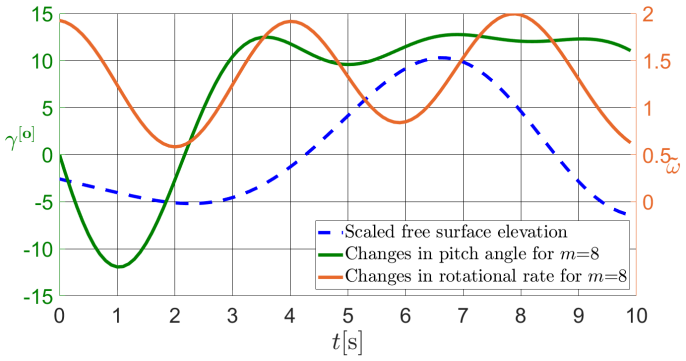


**FIGURE 6**. The solution for variable pitch and rotational rate for a cyclorotor with radius $R$=6m and submergence depth $D_s$=12m in panchromatic wave $T_e$=8s and $H$=1.5m.

Again, by way of example, Fig. 6 shows the solution for variable pitch and rotational rate for a cyclorotor with radius $R$ = 6m and submergence depth $D_s$ = 12m in the presented 10 seconds of a panchromatic wave with $T_e$ = 8s and $H_s$ = 1.5m. As a baseline, we note that, if the cyclorotor rotates with a constant optimal rotational velocity $\dot{\theta}_0$ = 0.3rad/s and neutral pitch angle $\gamma = 0^o$, it will generate just $P_{Shaft}$ = 0.6 kW/m while, after implementation of the real-time control strategy for $\dot{\theta}$ and $\gamma$, the generated power increases by a factor of more than 6, viz. $P_{Shaft}$ = 4.12kW/M.

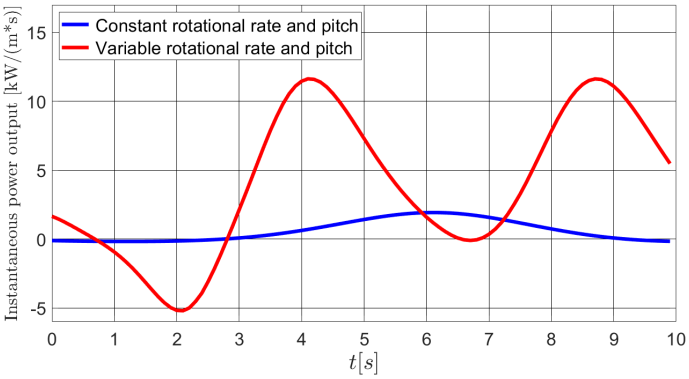


**FIGURE 7**. Increase in instantaneous power generation following implementation of the control strategy presented in Fig. 6.

For the panchromatic case, the optimal variations in pitch angle $\gamma$ and rotational rate $\dot{\theta}$ are quite significant, due to the stochastic and frequent changes in the speed and direction of the water particle motion in the path of the hydrofoils, constantly maintaining an optimal attack angle (and, as result, the lift coefficient) and rotational rate.

The angle of attack $\alpha$ is not only controlled using the foil pitch $\gamma$, but also using the rotational rate $\dot{\theta}$, with the incident water particle velocity vector as an unmeasured input. This type of control is not straightforward, since the tangential force $F_{T_i}$ is proportional to $|\hat{V}_i|^2$ (11) which, in turn, is related to the instantaneous foil velocity $V_{R_i}$ via (1). In contrast, the angle of attack $\alpha$ is inversely proportional to the instantaneous foil velocity $V_{R_i}$ (if $V_{R_i}$ is infinite, $\alpha$ and $C_L$ are zero). However, a decrease in rotational rate $\dot{\theta}$, to maintain an optimum stall attack angle (of $15^o$), may also decrease the rotor performance in terms of shaft power, since $P_{Shaft} \sim \dot{\theta}^3$ (12), (13). Thus, in some cases, the attack angle $\alpha$ can be decreased and, as result, decrease the lift coefficient $C_L(\alpha)$, but the rotational rate $\dot{\theta}$ of the cyclorotor will increase, with an overall increase in $P_{Shaft}$.

However, the optimal active pitch control strategy has a consistently positive effect on shaft power generation $P_{Shaft}$. In any event, the amount of parasitic energy expended for real time pitch control, and physical limitations on the hydrofoil pitch angle rate $\dot{\gamma}(t)$, require further investigation.

In terms of the sensitivity of mean converted shaft power to $D_s$ and $R$, for the panchromatic wave case, Tables 5 and 6 show the variations in $P_{Shaft}$ for corresponding changes in submergence depth $D_s$ and cyclorotor radius $R$. The reduced range of $D_s$ and $R$, compared to the monochromatic case, reflect the significantly increased computational demands of the panchromatic case, especially considering the need for a set of sea-state realisations to obtain statistically significant results. From Tables 5 and 6, two broad conclusions can be drawn:

(a) The captured mean power is relatively insensitive to variations in $D_s$ and $R$, compared to the monochromatic case, while
(b) In general, maximum values of $R$, and minimum values for $D_s$ are preferred, which are somewhat consistent with the results of Section 5.1

**TABLE 5**. Performance (kW/m), in terms of shaft power $P_{Shaft}$, in panchromatic waves for a twin-foil cyclorotor with a neutral pitch angle $\gamma = 0$ and constant rotational rate $\dot{\theta}_0 = 0.3$ rad/s for various values of submergence depth $D_s$ and radius $R$ in panchromatic waves with $T_e = 8$s and $H_s = 1.5$m.

| $D_s(m) \setminus R(m)$ | 5 | 6 | 7 | 8 |
|---|---|---|---|---|
| 11 | 0.41 | 0.68 | 0.89 | 1.1 |
| 12 | 0.43 | 0.6 | 0.78 | 0.96 |
| 15 | 0.3 | 0.41 | 0.51 | 0.6 |

**TABLE 6**. Performance (kW/m), in terms of shaft power $P_{Shaft}$, in panchromatic waves for a twin-foil cyclorotor with variable pitch angle $\gamma$ and variable rotational rate $\dot{\theta}$ for various values of submergence depth $D_s$ and radius $R$ in panchromatic waves with $T_e = 8$s and $H_s = 1.5$m.

| $D_s(m) \setminus R(m)$ | 5 | 6 | 7 | 8 |
|---|---|---|---|---|
| 11 | 3.35 | 4.28 | 6.39 | 11.9 |
| 12 | 3.15 | 4.12 | 6.04 | 8.65 |
| 15 | 2.85 | 3.65 | 4.6 | 7.99 |

## 6 Conclusions

This study aimed to examine the interplay between the 2 broad levels of the hierarchical control system presented in Fig.2. From the results presented in Section 5, it is clear that there is significant interaction between the two (fast and slow) control hierarchies, particularly for the monochromatic case. The results of Section 5.1 show a significant sensitivity in $P_{Shaft}$ to variations in $D_s$ and $R$, suggesting that the optimum $D_s$ and $R$ calculated for the optimal constant $\dot{\theta}$ and optimal constant $\gamma$ may not be optimal for the case where a variable $\dot{\theta}$ and $\gamma$ are employed. However, perhaps more meaningful conclusions can be drawn from the results of Section 5.2 (more realistic panchromatic waves), which show a broad monotonic increase in $P_{Shaft}$ with increasing $R$ and decreasing $D_s$. Therefore, the choice of the ideal $D_s$ and $R$ parameters for a particular wave site are likely to be determined by economic issues which balance the capital, and potential operational, cost of a large rotor against the energy receipts which incremental changes in $R$ bring. We note that, in general, given a particular optimal radius $R$, maximum power is captured by placing the cyclorotor as close to the surface as possible, subject to avoidance of harsh surface effects. Significant issues relating to structural loading on larger devices must also be considered.

A clear conclusion of this study, consistent with the results of [14] and [15], is that there is a significant benefit to the employment of a variable rotational rate $\dot{\theta}$, with potential improvement in captured power of average factor of 8, via the comparison of Tables 5 and 6. The situation regarding the use of a variable

pitch angle is perhaps not so crucial in monochromatic waves, providing that an optimised constant pitch (rather than a default neutral pitch) is employed.

However, for real sea-state variations, the optimal pitch angle will have some sensitivity to sea state and optimisation over a sea-state scatter plot for any target site is recommended (though computationally onerous). Fig.6 demonstrates that variable pitch can have a very useful benefit in panchromatic waves but also carries significant implementation issues. The use of a fixed pitch angle would significantly reduce reliability/maintenance issues, as well as a moderate reduction in capital cost and any parasitic energy consumption associated with the use of pitch actuators. Ultimately, a balance must be struck between the economic benefit (extra energy receipts) and detriment (increased capital cost, reduced reliability, parasitic energy consumption) of variable pitch angle. In addition, this study has assumed a relatively simple mechanism for pitch actuation, where $\gamma_1 = -\gamma_2 = \gamma$, consistent with some previous studies [13]. It is likely that, with the freedom of individual optimisation of $\gamma_1$ and $\gamma_2$, greater gains in captured energy could be achieved, but at greater penalties in reliability and capital cost. In addition, the control optimisation problem would become even more challenging with the increase in control space dimension.

This study has several limitations. One limitation is that the performance of the rotor, in terms of mechanical power $P_{Shaft}$, is not closely connected to the incoming wave power $P_{Wave}$. As a result, values of generated power exceeding the incoming wave power can be obtained for a rotor with large radius values (Table 4). This problem is the result of approximated lift and drag coefficients; specifically, the lift and drag coefficients $C_L, C_D$ [24] traditionally used for cyclorotor-based WEC performance assessment for the Atargis [13, 25] and LiftWEC [15] devices were obtained experimentally for *airfoils* in ideal conditions of an *air-tube*. In contrast, preliminary analysis of recent experiments in the wave flume of École Centrale de Nantes (ECN), France [26, 27] have shown that rotating hydrofoils in water experience quite significant drag and energy losses due to radiation damping (the rotor expends additional energy in radiating waves).

A further limitation relates to the nature of the nonlinear model (see Section 3 and [18]) used for simulation and, in particular, solution for the optimal control parameters. The use of this model, while computationally efficient compared to, say, a CFD model, results in a non-convex optimisation problem for the control parameters, with a consequent limitation in the number of cases (i.e. span of $R$ and $D_s$ values) that can be examined. Therefore, the results presented in Section 5 do not allow comprehensive conclusions to be drawn; rather the results should be considered as indicative. The difficulty in solving the control optimisation problem also has implications for any attempt to implement real-time control in an experimental setting; however, this is the subject a a separate research effort.

## ACKNOWLEDGEMENTS

This project has received funding from the European Union's Horizon 2020 research and innovation programme under (LiftWEC) grant agreement No. 851885. As always, the authors are grateful for useful discussion with other LiftWEC consortium members, including Abel Arredondo-Galeana, Paul Lamont-Kane, Matt Folley, Gerrit Olbert, Remy Pascal, Grégory Payne and Florent Thiebaut, and grateful for the support of the Irish Centre for High-End Computing (ICHEC).

## REFERENCES

[1] Babarit, A., and Clément, A. H., 2006. "Optimal latching control of a wave energy device in regular and irregular waves," *Applied Ocean Research,* ***28***(2), pp. 77–91.

[2] Ringwood, J. V., Bacelli, G., and Fusco, F., 2014. "Energy-maximizing control of wave-energy converters: The development of control system technology to optimize their operation," *IEEE control systems magazine,* ***34***(5), pp. 30–55.

[3] Ermakov, A., and Ringwood, J. V., 2021. "Rotors for wave energy conversion—practice and possibilities," *IET Renewable Power Generation (Special Issue on Wave Energy Conversion)*.

[4] Folley, M., and Whittaker, T., 2019. "Lift-based wave energy converters – an analysis of their potential," In 13th European Wave and Tidal Energy Conference, Napoli, Italy.

[5] Chozas, J., Tetu, A., and Arredondo-Galeana, A., 2021. "A parametric cost model for the initial techno-economic assessment of lift-force based wave energy converters," In Proceedings of 14th European Wave and Tidal Energy Conference, paper #2005, Plymouth, UK.

[6] Folley, M., and Lamont-Kane, P., 2021. "Optimum wave regime for lift-based wave energy converters," In Proceedings of 14th European Wave and Tidal Energy Conference, paper #1914, Plymouth, UK.

[7] Lamont-Kane, P., Folley, M., Frost, C., and Whittaker, T., 2021. "Preliminary investigations into the hydrodynamic performance of lift based wecs," In Proceedings of 14th European Wave and Tidal Energy Conference, paper #2074, Plymouth, UK.

[8] Hermans, A., Van Sabben, E., and Pinkster, J., 1990. "A device to extract energy from water waves," *Applied Ocean Research,* ***12***(4), pp. 175–179.

[9] Scharmann, N., 2014. "Ocean energy conversion systems: the wave hydro-mechanical rotary energy converter,", PhD thesis, PhD Thesis, Institute for Fluid Dynamics and Ship Theory, TUHH, Hamburg, Germany.

[10] Siegel, S. G., Fagley, C., Römer, M., and McLaughlin, T., 2012. "Experimental investigation of irregular wave cancellation using a cycloidal wave energy converter," In Proc. Intl. Conf. on Offshore Mechanics and Arctic Eng. (OMAE), Rio de Janeiro, Vol. 44946, American Society of Mechanical Engineers, pp. 309–320.

[11] Fagley, C. P., Seidel, J. J., and Siegel, S. G., 2012. "Computational investigation of irregular wave cancellation using

a cycloidal wave energy converter," In Intl. Conf. on Offshore Mechanics and Arctic Eng. (OMAE), Rio de Janeiro, Vol. 44946, American Society of Mechanical Engineers, pp. 351–358.

[12] Fagley, C. P., Seidel, J. J., and Siegel, S. G., 2012. "Wave cancellation experiments using a 1:10 scale cycloidal wave energy converter," In Proc. 1st Asian Wave and Tidal Energy Conference, Jeju Island, Korea.

[13] Siegel, S. G., 2019. "Numerical benchmarking study of a cycloidal wave energy converter," *Renewable Energy,* ***134***, pp. 390–405.

[14] Ermakov, A., Marie, A., and Ringwood, J., 2021. "Some fundamental results for cyclorotor wave energy converters," *IEEE Transactions on Sustainable Energy*, p. (Submitted).

[15] Ermakov, A., Marie, A., and Ringwood, J. V., 2022. "Optimal control of pitch and or rotational velocity for a cyclorotor wave energy device," *IEEE Transactions on Sustainable Energy*, p. (Submitted).

[16] Arredondo-Galeana, A., Shi, W., Olbert, G., Scharf, M., Ermakov, A., Ringwood, J. V., and Brennan, F., 2021. "A methodology for the structural design of liftwec: A wave-bladed cyclorotor," In 14th European Wave and Tidal Energy Conference, paper #1967, Plymouth, UK.

[17] Ermakov, A., and Ringwood, J. V., 2021. "Development of an analytical model for a cyclorotor wave energy device," In 14th European Wave and Tidal Energy Conference, paper #1885, Plymouth, UK.

[18] Ermakov, A., and Ringwood, J. V., 2021. "A control-orientated analytical model for a cyclorotor wave energy device with n hydrofoils," *Journal of Ocean Engineering and Marine Energy*, pp. 1–10.

[19] Ermakov, A., and Ringwood, J. V., 2021. "Erratum to: A control-orientated analytical model for a cyclorotor wave energy device with n hydrofoils," *Journal of Ocean Engineering and Marine Energy,* ***7***, p. 493–494.

[20] Dawson, H. G., 1897. "On the numerical value of $\int_0^h e^{x^2}\,dx$," *Proceedings of the London Mathematical Society,* ***s1-29 (1)***, pp. 519–522.

[21] Storn, R., and Price, K., 1997. "Differential evolution – a simple and efficient heuristic for global optimization over continuous spaces," *Journal of Global Optimization,* ***11***, pp. 341–359.

[22] Endres, S., Sandrock, C., and Focke, W., 2018. "A simplicial homology algorithm for lipschitz optimisation," *Journal of Global Optimization,* ***72***, pp. 181–217.

[23] Fagley, C., Mohtat, A., Chitale, K., and Siegel, S., 2021. "Dynamic estimation and control of a cycloidal wave energy converter in three-dimensional sea states," In Proceedings of 14th European Wave and Tidal Energy Conference, paper #2120, Plymouth, UK.

[24] Sheldahl, R., and Klimas, P., 1981. *Aerodynamic characteristics of seven symmetrical airfoil sections through 180-degree angle of attack for use in aerodynamic analysis of vertical axis wind turbines*. Sandia National Labs., Albuquerque.

[25] Siegel, S., 2014. "Wave climate scatter performance of a cycloidal wave energy converter," *Applied Ocean Research,* ***48***, pp. 331–343.

[26] Thiebaut, F., and Payne, G. Liftwec project: D4.4 report on physical modelling of 2d liftwec concepts. (accessed december 17, 2021). https://liftwec.com/d4-4-report-on-physical-modelling-of-2d-liftwec-concepts/.

[27] Thiebaut, F., Payne, G., Haquin, S., Web, M., Lambert, S., and Pettinotti, B. Liftwec project: D4.3 open access experimental data from 2d scale model. (accessed december 17, 2021). https://doi.org/10.5281/zenodo.5534471.